Journal of Materials Chemistry A

COMMUNICATION

View Article Online
View Journal | View Issue

A simple, low-cost CVD route to thin films of $BiFeO_3$ for efficient water photo-oxidation†

Cite this: *J. Mater. Chem. A*, 2014, **2**, 2922

Received 21st November 2013
Accepted 19th December 2013

DOI: 10.1039/c3ta14824f

www.rsc.org/MaterialsA

Savio J. A. Moniz,[ab] Raul Quesada-Cabrera,[a] Christopher S. Blackman,*[a] Junwang Tang,[b] Paul Southern,[c] Paul M. Weaver[d] and Claire J. Carmalt[a]

A novel method for preparation of $BiFeO_3$ films *via* a simple solution-based CVD method is reported using for the first time a single-source heterobimetallic precursor $[CpFe(CO)_2BiCl_2]$. $BiFeO_3$ films display ferroelectric and ferromagnetic ordering at room temperature and possess direct band-gaps between 2.0 and 2.2 eV. Photocatalytic testing for water oxidation revealed high activities under UVA (365 nm) and simulated solar irradiation, superior to that exhibited by a commercial standard (Pilkington Activ® TiO_2 film) resulting in an apparent quantum yield of ~24%.

Introduction

Water photolysis for H_2 fuel generation has the potential to meet increasing energy demands whilst reducing the emission of harmful greenhouse gases into the atmosphere. Water photolysis can be considered to be composed of two half reactions, water oxidation (to O_2) and water reduction (to H_2). However, water oxidation is widely considered to be more challenging given the fact that generation of one molecule of O_2 requires four holes, generated on a timescale five orders of magnitude slower than the two electron proton reduction to H_2.[1,2] Therefore the search for a stable, efficient water oxidation photocatalyst is widely regarded to be significant for large-scale water photolysis. The most commonly used materials for photocatalytic water splitting are binary transition metal oxides but the band-gaps of these materials (over 3.0 eV) are too high to serve as efficient photocatalysts under visible light irradiation.[3,4] Perovskite bismuth ferrite ($BiFeO_3$, "BFO") exhibits a direct band-gap of approximately 2.2 eV and is an active photocatalyst;[5–7] $BiFeO_3$ nanowires have been demonstrated to be promising oxygen evolution catalysts exhibiting high efficiencies under UV-light irradiation, and very recently Au–$BiFeO_3$ nanowires have been reported to be highly active for oxygen evolution under visible light ($\lambda > 380$ nm) irradiation.[8,9]

Chemical Vapour Deposition (CVD) has many potential advantages for deposition of $BiFeO_3$ thin films including excellent substrate coverage, low-cost, ease of scale-up, control over thickness and morphology and high throughput capabilities, however the growth of phase-pure $BiFeO_3$ films using chemical deposition techniques is challenging.[10–12] It has been suggested that single-source heterometallic precursors could be exploited in order to improve stoichiometry control in multi-component materials.[12,13] However no examples for $BiFeO_3$ thin films appear in the literature despite the availability of a number of bimetallic bismuth-iron containing complexes, *i.e.* $[Bi_2(Hsal)_6{\cdot}M(acac)_3]$ (M = Al, V, Cr, Fe, Co)[14] and $[Bi_2M(hfac)_8]$ (M = Mn, Fe, Co, Ni, Cu, Zn)[15] which could serve as potential precursors. Here, we describe the growth of $BiFeO_3$ films onto a variety of substrates *via* a simple, low-cost solution based aerosol assisted (AA)CVD process utilizing the single-source precursor $[CpFe(CO)_2BiCl_2]$ (Cp = cyclopendienyl, C_5H_5). AACVD is advantageous as it does not rely upon the use of highly volatile precursors, essential for typically high molecular weight heterometallic cluster compounds.[16] Post-deposition heat treatment of as-deposited films resulted in pure $BiFeO_3$ at 700 °C, confirmed *via* XRD, low temperature Raman and XPS spectroscopy. $BiFeO_3$ films displayed the expected ferroelectric and ferromagnetic behavior and possessed direct band-gaps of ~2.1 eV and we have demonstrated the films to be highly active photocatalysts for water oxidation under simulated solar irradiation. This new synthetic methodology enables large area thin

[a]*Materials Chemistry Centre, Department of Chemistry, University College London, 20 Gordon Street, London, WC1H 0AJ, UK. E-mail: c.blackman@ucl.ac.uk*
[b]*Department of Chemical Engineering, University College London, Torrington Place, London, WC1E 7JE, UK*
[c]*UCL Healthcare Biomagnetics Laboratories, 21 Albemarle Street, London, W1S 4BS, UK*
[d]*National Physical Laboratory, Hampton Road, Teddington, Middlesex, TW11 0LW, UK*

† Electronic supplementary information (ESI) available: Further experimental details, DSC–TGA pattern of $[\{Cp(CO)_2Fe\}BiCl_2]$, Raman spectrum of a pure $BiFeO_3$ film recorded at −195 °C, XPS spectrum of the Fe 2p region of a $BiFeO_3$ thin film after etching, top-down SEM images of $Bi_{24}Fe_2O_{39}$ film deposited on glass at 300 °C, top-down SEM images of the films annealed between 400 and 650 °C, P–E hysteresis loop for a pure $BiFeO_3$ film on $Pt/SiO_2/Si$ substrate, M–H and ZFC–FC curves for $BiFeO_3$ film, UV-vis spectrum of a pure $BiFeO_3$ film, corresponding Tauc plot for a $BiFeO_3$ film. See DOI: 10.1039/c3ta14824f

film deposition, and hence is relevant for high volume applications such as solar driven water oxidation or organic pollutant degradation for water treatment.

Experimental

Detailed experimental information on film analysis and photochemical measurements are provided in ESI.†

Precursor synthesis

The bimetallic molecular precursor $[\{Cp(CO)_2Fe\}BiCl_2]$ was synthesised according to the literature from a simple equimolar reaction of $[CpFe(CO)_2]_2$ and $BiCl_3$ in dichloromethane, and possessed identical NMR and IR spectra to those previously reported.[17]

CVD

AACVD reactions were carried out using an in-house built cold-wall CVD described elsewhere.[18,19] Nitrogen (99.96%) was obtained from BOC and used as supplied. AACVD experiments were initially conducted on SiCO cated float glass substrates (150 mm × 45 mm × 3 mm) supplied by Pilkington Glass Ltd (NSG group). The glass substrates were cleaned thoroughly in commercial washing up detergent, dried, and then cleaned with isopropanol then dried using a heat gun. In order to anneal films to temperatures greater than 600 °C, depositions were carried out on 20 mm × 20 mm × 2 mm Corning 1737 AMLCD alkaline-earth boro-aluminosilicate transparent glass substrates. For ferroelectric measurements, films were deposited onto silicon wafers which were sputtered for 180 seconds with a thin layer of platinum (argon pressure 0.1 torr, current 25 mA) prior to use, with film deposition onto the platinum. 150 mg (0.33 mmol) of $[CpFe(CO)_2BiCl_2]$ precursor dissolved in *ca.* 40 cm^3 dry THF was used for each deposition. The nitrogen gas flow through the precursor was maintained at 0.8 l min^{-1} and regulated using a calibrated flow meter. Annealing was carried out in air for two hours at a heating ramp rate of 10 °C min^{-1}. For each annealing experiment a fresh sample deposited *via* AACVD at a substrate temperature of 300 °C was used.

Photoelectrochemical measurements

Chronoamperometry measurements were conducted using a potentiostat, a Pyrex cell with a glass window and a mechanical light chopper. A Pt wire was used as the counter electrode and an Ag/AgCl electrode was used as the reference electrode. An aqueous 0.2 M sodium sulphate (Na_2SO_4) solution was purged for 15 minutes with argon and was used as the electrolyte (pH 6.5). The light source was a 150 W Xe lamp equipped with an AM 1.5G filter (100 mW cm^{-2}, 1 Sun, Newport, USA). The cell was sealed with a rubber septum. The scan rate was 10 mV s^{-1}. Mott–Schottky (impedance) measurements were measured in 0.2 M Na_2SO_4 in the dark at a frequency of 1 kHz and scan rate of 10 mV s^{-1}. The potential was measured against an Ag/AgCl reference electrode and converted to RHE potentials using $E(\text{RHE}) = E(\text{Ag/AgCl}) + (0.059 \times \text{pH}) + 0.197$ V.

Photocatalytic oxygen evolution

Selected films were used to photo-oxidise water using sacrificial reagents (alkaline sodium persulphate) under UVA (365 nm) and simulated solar irradiation (150 W Xe lamp).[20] In a typical experiment, the film was immersed in 30 cm^3 aqueous solution under strong stirring conditions (55 rpm) in a quartz vessel with water-cooled walls ($T = 298$ K). The photo-oxidation of water is biased through immersion in a solution containing a sacrificial electron–acceptor (scavenger) composed of 0.01 M $Na_2S_2O_8$ in 0.1 M NaOH.[21] The MPD is comprised of a circular shaped silver electrode (counter and reference) and a platinum electrode disc (cathode) connected *via* a salt bridge (3 M KCl).[21] The Pt electrode is protected from the test solution by a gas-permeable PTFE membrane.

Results and discussion

AACVD of $[CpFe(CO)_2BiCl_2]$ (the TGA trace of this compound is shown in the ESI, Fig. S1†) in THF solvent at a substrate temperature of 300 °C resulted in the formation of adherent dark orange films, passing the Scotch tape test, with complete substrate coverage. Compositional analysis *via* WDX revealed these films contained 74 at% bismuth, 23 at% iron and 3 at% chlorine. X-ray diffraction showed only the presence of $Bi_{24}Fe_2O_{39}$ (Fig. 1(a), $a = b = 7.28\,(4)$ Å, $c = 5.67(2)$ Å, $\alpha = \beta = \gamma = 90°$, space group $P\bar{4}21c$, PDF no. 042-0201), indicating other

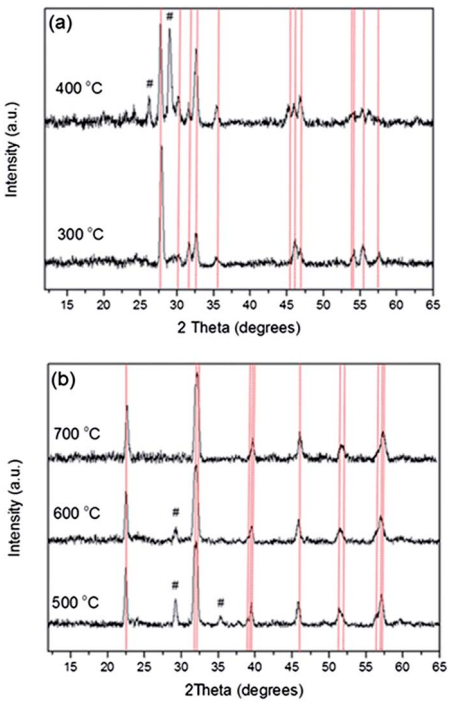

Fig. 1 (a) X-ray diffraction patterns of BFO films annealed at 300 °C (as-deposited) and 400 °C. Red lines correspond to $Bi_{24}Fe_2O_{39}$ (PDF = 042-0201). (b) X-ray diffraction patterns of films annealed at temperatures between 500 and 700 °C. Red lines correspond to $BiFeO_3$ (PDF = 014-0181). # corresponds to $Bi_2Fe_4O_9$ (PDF = 025-0090).

non-crystalline iron or bismuth rich species must also be present. No evidence of $BiFeO_3$ formation was observed at this temperature (300 °C) *via* X-ray diffraction. XPS analysis revealed the presence of Fe $2p_{3/2}$ at 710.9 eV and Bi $4f_{7/2}$ at 158.7 eV, characteristic of the presence of Fe^{3+} and Bi^{3+}.[22,23] In order to obtain $BiFeO_3$ the as-deposited films were annealed at a variety of temperatures up to 700 °C (between 450 and 550 °C Pilkington SiCO float glass was used and for 700 °C Corning glass was used) with the average results, after repeating the process several times to ensure reproducibility, summarised in Table 1.

Post-deposition annealing at increasing temperature led to a decrease in film thickness and relative loss of bismuth (to iron), most likely as bismuth or bismuth oxide,[24] and progressive conversion of $Bi_{24}Fe_2O_{39}$ to $Bi_2Fe_4O_9$ and subsequently to $BiFeO_3$ in agreement with the phase diagram constructed by Scott[25] and Lu.[26] Raising the annealing temperature to 700 °C caused the Bi : Fe ratio to become near unity (Bi 51 at%, Fe 49 at%) and the appearance of the films changed from dark orange (as-deposited) to bright orange. At 700 °C $BiFeO_3$ was the only phase present *via* XRD [Fig. 1(b), $a = b = 5.588(4)$ Å, $c = 13.913$ (6) Å, space group $R3c$, bulk $BiFeO_3$ $a = b = 5.57414$ (4) Å, $c = 13.85882$ (12) Å, PDF = 014-0181].[27] Raman analysis further confirmed the assignment of phase pure $BiFeO_3$ (ESI, Fig. S2†). Chlorine contamination from the precursor was initially high for the as-deposited film and for those annealed at 400 °C (2.5 and 1.6 at% respectively), however this contamination decreased dramatically as a function of annealing temperature and by 600 °C was below the detection limit of WDX.

XPS of a film annealed at 700 °C showed the presence of iron in the +3 oxidation state [Fe $2p_{3/2}$, 711.3 eV (Fig. S3, ESI†)] with the expected Fe^{3+} satellite peak observed at 718.9 eV.[12] Oxygen under stoichiometry, leading to a co-existence of Fe^{2+} and Fe^{3+} species, leads to broadening of the Fe $2p_{3/2}$ peak to lower energies but this was not observed in our samples. A single Bi $4f_{7/2}$ ionisation at 159.4 eV was observed, characteristic of bismuth in the +3 oxidation state, as expected for $BiFeO_3$.[23] No chlorine contamination was detected *via* XPS; carbon was observed on the surface but decreased upon etching indicating it to be surface contamination. Analysis of the Bi 4f, Fe 2p and O 1s (B.E. of O 1s = 530.2 eV) peak areas after etching indicated the presence of the three components in an approximate 1 : 1 : 3 ratio, commensurate with $BiFeO_3$.

As-deposited films (300 °C) possessed a globular morphology, with average particle diameters of 100 nm (ESI, Fig. S4†). Heat treatment at higher temperatures led to coalescence of particles (ESI, Fig. S5†), whilst at 700 °C (Fig. 2(a)) the sintering of the particles led to films becoming rougher and less uniform; AFM (Fig. 2(c and d)) showed the films to be comprised of larger aggregates with a rough texture (root mean squared roughness (rms) = 62 nm) in agreement with SEM. Hence films synthesised by this route are likely to possess high surface areas for enhanced catalytic activity.

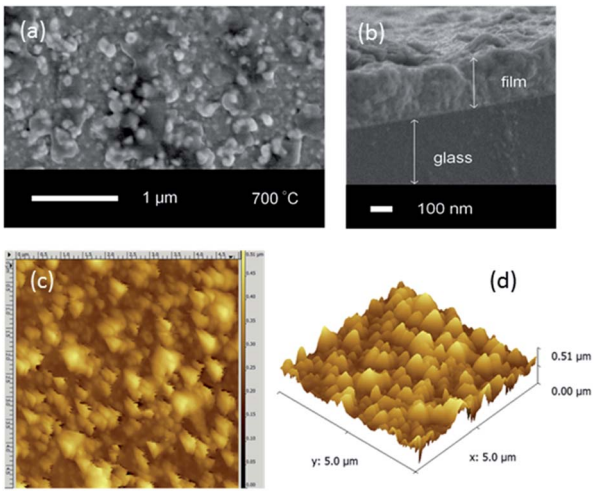

Fig. 2 (a) A typical top-down SEM image (b) side-on SEM image, (c) a 5 μm field size AFM image and (d) the corresponding 3D AFM image of the $BiFeO_3$ film formed after annealing at 700 °C.

Films of $BiFeO_3$, grown by deposition directly onto 1 cm^2 Pt/SiO_2/Si wafers *via* AACVD followed by annealing at 700 °C, displayed a maximum polarisation of 8.7 μC cm^{-2}, providing an effective relative permittivity of almost 800 (ESI, Fig. S6†). The maximum polarisation is smaller than that for single crystal or epitaxial film bismuth ferrite (around 50 μC cm^{-2}),[28] but higher than those obtained for $BiFeO_3$ films grown *via* sol–gel processing (P_r = 1.8 μC cm^{-2})[29] or PLD (P_r = 0.83 μC cm^{-2}).[30] Measurement of the magnetic properties of a 320 nm thick film (ESI, Fig. S7†) revealed that the M–H hysteresis loops recorded at 5 K and 300 K were similar to those reported previously[28] (after subtracting the diamagnetic contribution from the substrate), *i.e.* these $BiFeO_3$ films show weak ferromagnetic behaviour with well-saturated hysteresis loops at both temperatures. Upon raising the temperature to 300 K the coercivity was measured as 135 Oe and −115 Oe with an expected decrease in saturation magnetisation to 8.9 emu cm^{-3}. The coercivity is lower than that observed for a 70 nm thick $BiFeO_3$ film grown *via* PLD (200 Oe)[31] although a decrease in magnetisation as a

Table 1 Details of the deposition and main annealing conditions

Annealing temp. °C	Phase(s) obtained *via* XRD	At% Bi : Fe (from WDX)	Av. film thickness/ nm	Band-gap/ eV	At% Cl contamination (from WDX)
300 (as deposited)	$Bi_{24}Fe_2O_{39}$	74 : 23	1700	n/a	3
400	$Bi_{24}Fe_2O_{39}$ + $Bi_2Fe_4O_9$	60 : 38	1580	n/a	2
500	$BiFeO_3$ + $Bi_2Fe_4O_9$	58 : 41	1110	2.0	<1
600	$BiFeO_3$ + $Bi_2Fe_4O_9$	53 : 47	680	2.2	0
700	$BiFeO_3$	51 : 49	320	2.1	0

function of increasing film thickness was observed, from 150 emu cm^{-3} for a 70 nm thick film to 5 emu cm^{-3} for a 400 nm thick film, consistent with our measurement of film thickness (~320 nm). Spin-glass behaviour was also observed from M–T measurements (ESI†).

A typical transmission spectrum of a film containing $BiFeO_3$ as the only crystalline phase (ESI, Fig. S8†) shows over 70% transmittance in the 800–2500 nm range with the cut-off from the glass substrate coming into effect below 380 nm. The band-gaps of the films were calculated using Tauc plots (see Fig. S9, ESI†).[32] Extrapolating the linear part of the plot to the *x*-axis for a phase-pure sample resulted in an intercept of approximately 2.1 eV, in good agreement with experimentally derived band-gap values for $BiFeO_3$; films with smaller band-gaps (2.0 eV) contained impurity $Bi_2Fe_4O_9$ and are in line with the expected decrease in band-gap of $Bi_2Fe_4O_9$ compared to $BiFeO_3$.[33,34]

For photoelectrochemical (PEC) measurements $BiFeO_3$ was grown on FTO coated glass substrates. In order to estimate the relative levels of the conduction and valence bands of $BiFeO_3$ electrical impedance measurements were carried out from which the flat-band potential (E_{fb}) was measured. Fig. 3(a) displays the Mott–Schottky plot for a $BiFeO_3$ film deposited onto FTO coated glass. For n-type semiconductors the flat-band potential (E_{fb}) is considered to be located just under the conduction band, hence E_{fb} of $BiFeO_3$ was estimated to be −0.31 V (*vs.* Ag/AgCl) or + 0.18 V (*vs.* RHE),[35,36] which is similar to values previously estimated from atomic electronegativities.[37] Based upon this value and that determined for the band-gap of $BiFeO_3$ (2.1 eV), a band diagram (Fig. 3(b)) was constructed, indicating $BiFeO_3$ has significant overpotential for photocatalytic water oxidation.

The photoanodic activity of $BiFeO_3$ was investigated using PEC measurements and also *via* oxygen evolution using a sacrificial electron acceptor solution. Fig. 4 shows the chronoamperometry measurement obtained from a $BiFeO_3$ photoelectrode under 1 Sun (100 mW cm^{-2}) AM 1.5G illumination. There is a steady increase in photocurrent with increasing potential and the photocurrent at 1.0 V *vs.* Ag/AgCl was appreciable (*ca.* 0.1 mA cm^{-2} (103 μA cm^{-2})). This value is similar to that obtained by Yu *et al.*[38] for $BiFeO_3$ films deposited *via* PLD onto platinised silicon substrates (~90 μA cm^{-2} at 1.0 V *vs.* Ag/AgCl, 400 W Xe lamp) but substantially higher than the current density reported for hydrothermally synthesised $BiFeO_3$ nanocube electrodes in pure water (5.2 μA cm^{-2} at 1.0 V *vs.* SCE, 500 W Hg lamp)[39] and higher than BFO/SRO/STO films grown *via* sputtering (10 μA at 0.64 V *vs.* Ag/AgCl).[40]

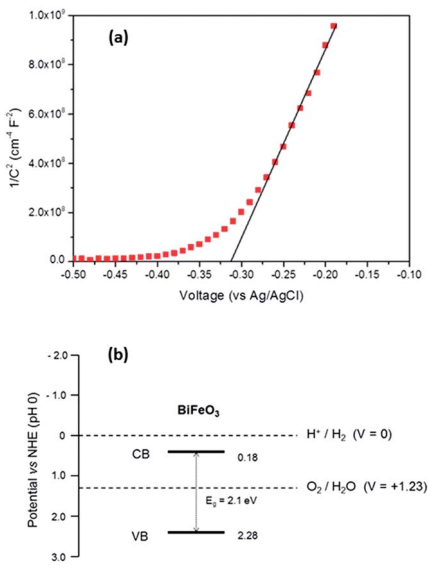

Fig. 3 (a) Mott–Schottky plot for $BiFeO_3$ electrode measured in the dark using 0.2 M Na_2SO_4 at pH 6.5, (b) schematic illustration of the estimated location of the conduction and valence bands in $BiFeO_3$ with respect to the redox potentials of water splitting.

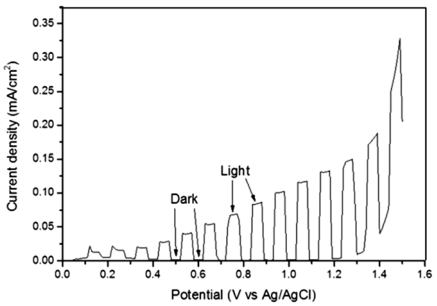

Fig. 4 *I–V* curve for a $BiFeO_3$ film deposited on FTO glass *via* AACVD.

In order to verify the water oxidation activity, tests for oxygen evolution from a $Na_2S_2O_8$/NaOH sacrificial solution were carried out using an MPD cell (see ESI† for more details) and compared to a commercial standard photocatalyst (Pilkington Activ® glass).[41] The overall photocatalytic reaction is given by eqn (1).

$$2S_2O_8^{2-} + 2H_2O \rightarrow 4SO_4^{2-} + 4H^+ + O_2 \quad (1)$$

Fig. 5 shows the typical output of the MPD cell during photogeneration of oxygen on $BiFeO_3$ films under full-arc Xe-lamp irradiation (150 W) with the corresponding amounts of oxygen produced during the first 10 h irradiation shown in Fig. 5(b). The output reading shows an increase in voltage during an initial illumination period followed by a plateau around 0.05 V, indicating steady oxygen production during prolonged irradiation (above 20 h). A small drop in the signal when turning on the Xe lamp, attributed to an interruption of the electrical supply, was observed however this did not affect the observed rate. Signal drift was also observed after prolonged use of the MPD cell, as illustrated by the blank test carried out on uncoated glass, however signal drop was noted after switching off the light source demonstrating the oxygen evolution was a photocatalytic effect. In addition no change in voltage, *i.e.* no oxygen evolution, was observed in the absence of illumination. The oxygen rates and % O_2 yields obtained during UVA irradiation of $BiFeO_3$ and Activ® glass films are given in Table 2.

The % O_2 yield of the process has been determined according to eqn (2).

$$\%\ O_2\ \text{yield} = (\text{molecules formed/incident photons}) \times 4\ (\text{electrons}) \times 100\% \quad (2)$$

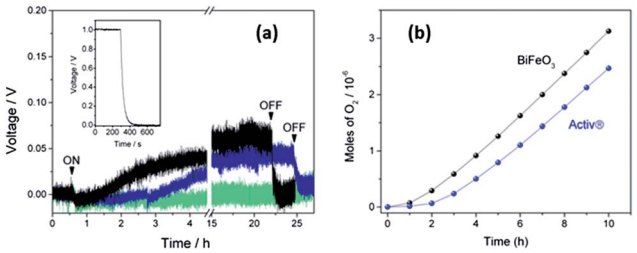

Fig. 5 (a) Typical output of the MPD cell during photo-generation of oxygen on $BiFeO_3$ (black line) and Activ glass (blue line) films under solar (Xe) lamp irradiation conditions. The shaded areas represent running time in the dark. A test using a plain glass substrate is also included for reference (green line). The inset shows the typical output signal for air- and nitrogen-saturation conditions (1 and 0 V, respectively); (b) continuous oxygen evolution of both $BiFeO_3$ and TiO_2 (Activ) films under solar irradiation over a period of 10 hours.

Table 2 Rates of oxygen under different (full-arc Xe lamp and blacklight UVA) irradiation conditions and efficiencies and oxygen yields for experiments under UVA light (1.5 mW cm^{-2})

	Rate of O_2 evolution (μmol h^{-1})		O_2 yield
	Solar lamp	UVA	(%, 365 nm)
$BiFeO_3$	0.33	0.023	24.4
TiO_2 (Activ)	0.26	0.012	4.8

An average O_2 yield of 24.4% (365 nm) was obtained for $BiFeO_3$ (in the absence of co-catalyst) which represents a near 10-fold increase over optimised B-doped TiO_2 films investigated under identical conditions.[42] The O_2 yield of the Activ® reference was ~5% at 365 nm. It should be noted that the $BiFeO_3$ films tested were significantly thicker (~300 nm) than that reported for the TiO_2 layer in Activ® glass (~15 nm). XPS and X-ray diffraction patterns of the films conducted after photocatalytic testing revealed no change in composition or phase indicating that these $BiFeO_3$ films are robust under the basic conditions of the test and do not undergo photocorrosion, which was supported by the continued measurement of oxygen evolution on prolonged irradiation and subsequent tests which proved the effect was reproducible. Visible-light tests were also carried out using UV cut-off filters under similar experimental conditions however no increase in voltage could be distinguished above the signal drift of the MPD cell. This is perhaps not surprising given the photocatalytic activity of $BiFeO_3$ powders for oxygen evolution (from a $FeCl_3$ solution) using visible light irradiation (500 W Hg lamp, $\lambda > 420$ nm) is less than 0.2 μmol h^{-1},[39] and hence we are currently investigating more suitable methods for evaluating the visible light activity of $BiFeO_3$ thin films. The high photocatalytic activity for water oxidation displayed by our $BiFeO_3$ films may not be solely due to the high surface area of thin films; it has recently been reported that ferroelectric domains in $BiFeO_3$ enhance charge-carrier separation through photocatalytic decomposition of $AgNO_3$, resulting in selective Ag reduction on the surface and simultaneous oxygen evolution under visible light irradiation.[43,44]

Conclusions

For the first time, $BiFeO_3$ films were grown *via* a simple solution-based AACVD procedure at an unprecedented low temperature using the single-source precursor [{$Cp(CO)_2Fe$}$BiCl_2$], followed by post-deposition annealing at elevated temperature in air. As-deposited films were characterised as containing $Bi_{24}Fe_2O_{39}$ *via* XRD; annealed films were identified as $BiFeO_3$ by XRD and Raman spectroscopy with compositional analysis revealing bismuth to iron ratios of 1 : 1. Magnetic hysteresis and ferroelectric polarisation measurements confirmed ferromagnetic and ferroelectric ordering at room temperature. Direct band-gaps between 2.0 and 2.2 eV were measured for all films. Photocatalytic testing under both UV and solar irradiation confirmed appreciable activity of $BiFeO_3$ for the kinetically slow four hole process of water oxidation.[1] Despite having a less deep valence band potential than TiO_2, facile water oxidation is found, with the resultant apparent quantum yield of our samples exhibiting a near six-fold increase over a commercial standard photocatalyst (TiO_2 Activ® glass) and a ten-fold increase over B-doped TiO_2 films recently reported.[42] Furthermore, we have demonstrated the possibility of using relatively non-volatile molecular compounds for the growth of complex heterometallic oxides *via* AACVD. To the best of our knowledge, no precursors of this class have previously been utilised in CVD processes.

Acknowledgements

UCL/EPSRC are acknowledged for financial support. Dr Steve Firth is thanked for assistance with low temperature Raman spectroscopy. The NPL would like to acknowledge financial support from the UK's National Measurement system. Dr Emily Smith is thanked for XPS analysis under EPSRC grant EP/F019750/1: "A Coordinated Open-Access Centre for Comprehensive Materials Analysis".

Notes and references

1 J. Tang, J. R. Durrant and D. R. Klug, *J. Am. Chem. Soc.*, 2008, **130**, 13885–13891.
2 D. J. Martin, N. Umezawa, X. Chen, J. Ye and J. Tang, *Energy Environ. Sci.*, 2013, **6**, 3380–3386.
3 A. Bard and M. Fox, *Acc. Chem. Res.*, 1995, **28**, 141–145.
4 A. Kudo, K. Omori and H. Kato, *J. Am. Chem. Soc.*, 1999, **121**, 11459–11467.
5 F. Gao, X. Y. Chen, K. B. Yin, S. Dong, Z. F. Ren, F. Yuan, T. Yu, Z. G. Zou and J.-M. Liu, *Adv. Mater.*, 2007, **19**, 2889–2892.
6 S. Li, Y. Lin, B. Zhang and Y. Wang, *J. Phys. Chem. C*, 2010, **114**, 2903–2908.
7 X. Xu, Y.-H. Lin, P. Li, L. Shu and C.-W. Nan, *J. Am. Ceram. Soc.*, 2011, **94**, 2296–2299.

8 F. Gao, Y. Yuan, K. F. Wang, X. Y. Chen, F. Chen, J.-M. Liu and Z. F. Ren, *Appl. Phys. Lett.*, 2006, **89**, 102506.
9 S. Li, J. Zhang, M. G. Kibria, Z. Mi, M. Chaker, D. Ma, R. Nechache and F. Rosei, *Chem. Commun.*, 2013, **49**, 5856–5858.
10 S. Y. Yang, F. Zavaliche, L. Mohaddes-Ardabili, V. Vaithyanathan, D. G. Schlom, Y. J. Lee, Y. H. Chu, M. P. Cruz, Q. Zhan, T. Zhao and R. Ramesh, *Appl. Phys. Lett.*, 2005, **87**, 102903.
11 M. Kartavtseva, O. Gorbenko and A. Kaul, *Surf. Coat. Technol.*, 2007, **201**, 9149–9153.
12 J. Thery, C. Dubourdieu, T. Baron, C. Ternon, H. Roussel and F. Pierre, *Chem. Vap. Deposition*, 2007, **13**, 232–238.
13 A. C. Jones, *J. Mater. Chem.*, 2002, **12**, 2576–2590.
14 J. H. Thurston, D. Trahan, T. Ould-Ely and K. H. Whitmire, *Inorg. Chem.*, 2004, **43**, 3299–3305.
15 E. V Dikarev, H. Zhang and B. Li, *J. Am. Chem. Soc.*, 2005, **127**, 6156–6157.
16 P. Marchand, I. A. Hassan, I. P. Parkin and C. J. Carmalt, *Dalton Trans.*, 2013, **42**, 9406–9422.
17 T. Gröer and M. Scheer, *J. Chem. Soc., Dalton Trans.*, 2000, 647–653.
18 S. Vallejos, T. Stoycheva, P. Umek, C. Navio, R. Snyders, C. Bittencourt, E. Llobet, C. Blackman, S. Moniz and X. Correig, *Chem. Commun.*, 2011, **47**, 565–567.
19 S. J. A. Moniz, D. Bhachu, C. S. Blackman, A. J. Cross, S. Elouali, D. Pugh, R. Quesada Cabrera and S. Vallejos, *Inorg. Chim. Acta*, 2012, **380**, 328–335.
20 S. J. A. Moniz, C. S. Blackman, C. J. Carmalt and G. Hyett, *J. Mater. Chem.*, 2010, **20**, 7881–7886.
21 A. Mills and M. A. Valenzuela, *J. Photochem. Photobiol., A*, 2004, **165**, 25–34.
22 T. Yamashita and P. Hayes, *Appl. Surf. Sci.*, 2008, **254**, 2441–2449.
23 V. S. Dharmadhikari, S. Sainkar, S. Badrinarayan and A. Goswami, *J. Electron Spectrosc. Relat. Phenom.*, 1982, **25**, 181–189.
24 F. Tyholdt, S. Jørgensen, H. Fjellvåg and A. E. Gunnaes, *J. Mater. Res.*, 2005, **20**, 2127–2139.
25 R. Palai, R. Katiyar, H. Schmid, P. Tissot, S. Clark, J. Robertson, S. Redfern, G. Catalan and J. Scott, *Phys. Rev. B: Condens. Matter Mater. Phys.*, 2008, **77**, 1–11.
26 K. Feng, L.-C. Wang, J. Lu, Y. Wu and B.-G. Shen, *CrystEngComm*, 2013, **15**, 4900.
27 A. Reyes, C. Delavega, M. Fuentes and L. Fuentes, *J. Eur. Ceram. Soc.*, 2007, **27**, 3709–3711.
28 G. Catalan and J. F. Scott, *Adv. Mater.*, 2009, **21**, 2463–2485.
29 Y. Wang, Q. Jiang, H. He and C.-W. Nan, *Appl. Phys. Lett.*, 2006, **88**, 142503.
30 V. R. Palkar, J. John and R. Pinto, *Appl. Phys. Lett.*, 2002, **80**, 1628.
31 J. Wang, J. B. Neaton, H. Zheng, V. Nagarajan, S. B. Ogale, B. Liu, D. Viehland, V. Vaithyanathan, D. G. Schlom, U. V Waghmare, N. A. Spaldin, K. M. Rabe, M. Wuttig and R. Ramesh, *Science*, 2003, **299**, 1719–1722.
32 J. Tauc, R. Grigorovici and A. Vancu, *Phys. Status Solidi B*, 1966, **15**, 627–637.
33 D. Cai, D. Du, S. Yu and J. Cheng, *Procedia Eng.*, 2012, **27**, 577–582.
34 Q.-J. Ruan and W.-D. Zhang, *J. Phys. Chem. C*, 2009, **113**, 4168–4173.
35 K. Sayama, A. Nomura, T. Arai, T. Sugita, R. Abe, M. Yanagida, T. Oi, Y. Iwasaki, Y. Abe and H. Sugihara, *J. Phys. Chem. B*, 2006, **110**, 11352–11360.
36 S. J. Hong, S. Lee, J. S. Jang and J. S. Lee, *Energy Environ. Sci.*, 2011, **4**, 1781.
37 S. Li, Y.-H. Lin, B.-P. Zhang, J.-F. Li and C.-W. Nan, *J. Appl. Phys.*, 2009, **105**, 054310.
38 X. Y. Chen, T. Yu, F. Gao, H. T. Zhang, L. F. Liu, Y. M. Wang, Z. S. Li, Z. G. Zou and J.-M. Liu, *Appl. Phys. Lett.*, 2007, **91**, 022114.
39 U. A. Joshi, J. S. Jang, P. H. Borse and J. S. Lee, *Appl. Phys. Lett.*, 2008, **92**, 242106.
40 W. Ji, K. Yao, Y.-F. Lim, Y. C. Liang and A. Suwardi, *Appl. Phys. Lett.*, 2013, **103**, 062901.
41 A. Mills, A. Lepre, N. Elliott, S. Bhopal, I. P. Parkin and S. A. O'Neill, *J. Photochem. Photobiol., A*, 2003, **160**, 213–224.
42 P. Carmichael, D. Hazafy, D. S. Bhachu, A. Mills, J. A. Darr and I. P. Parkin, *Phys. Chem. Chem. Phys.*, 2013, **15**, 16788–16794.
43 Y. Zhang, A. M. Schultz, P. A. Salvador and G. S. Rohrer, *J. Mater. Chem.*, 2011, **21**, 4168–4174.
44 A. M. Schultz, Y. Zhang, P. A. Salvador and G. S. Rohrer, *ACS Appl. Mater. Interfaces*, 2011, **3**, 1562–1567.